(w/v). X-ray scattering, density, DSC, and surface epoxidation show that the gel and single lamellas have the same crystalline structure, crystalline stem length, and crystallinity. Transmission electron microscopy established that the gel is a connected lamellar structure. On the basis of the average fold length of 16 monomer units for 89% *trans*-PBD, a "fold entanglement" mechanism of gelation is proposed.

4. About 5% of the cis units in the 10% cis-containing polybutadiene enter the crystalline core of the lamellas. This leads to a much lower transition temperature, melting point, and enthalpy of fusion than that measured for the 1:99 *cis*-/*trans*-polybutadiene.

Acknowledgment. We wish to thank S. D. Wang for his X-ray scattering results. This work was supported by the PSC/CUNY Faculty Research Award Program.

Registry No. Polybutadiene, 9003-17-2.

References and Notes

(1) Wang, P.; Woodward, A. E. *Macromolecules* **1987**, *20*, 1818.
(2) Schilling, F. C.; Bovey, F. A.; Tseng, S.; Woodward, A. E. *Macromolecules* **1983**, *16*, 808.
(3) Wang, P.; Woodward, A. E. *Macromolecules* **1987**, *20*, 1823.
(4) Clague, A. D. H.; Von Broekhoven, J. A. M.; Blaauw, L. P. *Macromolecules* **1974**, *7*, 348.
(5) Keller, A. In *Polymers, Liquid Crystals, and Low-Dimensional Solids*; March, N., Tosi, M., Eds.; Plenum: New York, 1984; Chapter 3.
(6) Pakula, T. *Polymer* **1983**, *23*, 1300.
(7) Domszy, R. C.; Alamo, R.; Edwards, C. O.; Mandelkern, L. *Macromolecules* **1986**, *19*, 310.
(8) Sanchez, I. C.; Eby, R. K. *Macromolecules* **1975**, *8*, 638.
(9) Grebowicz, J.; Aycock, W.; Wunderlich, B. *Polymer* **1986**, *27*, 575.

Structural Change Accompanying Volume Change in Amorphous Polystyrene As Studied by Small and Intermediate Angle X-ray Scattering

Hyun-Hoon Song and Ryong-Joon Roe*

Department of Materials Science and Engineering, University of Cincinnati, Cincinnati, Ohio 45221-0012. *Received April 3, 1987*

ABSTRACT: X-ray intensities scattered at small and intermediate angles from amorphous polystyrene were measured to study the change in the structure of the material as its volume was altered by five different methods. The volume changes were effected by (i) temperature change above T_g, (ii) temperature change below T_g, (iii) densification by application of pressure above T_g and subsequent release of the pressure at room temperature, (iv) spontaneous volume expansion of the pressure-densified material, and (v) spontaneous volume contraction on isothermal annealing below T_g (physical aging). The intensity data were examined either directly or after transformation into the density fluctuation function, the latter evaluated as a function of the size of the region of interest. The results show that the large scale density fluctuation correlates fairly well with the change of specific volume, irrespective of the different methods used to induce it. On the other hand, the small scale density fluctuation, indicating the degrees of local ordering, depends very sensitively on the method of volume change employed. In particular, (a) the volume contraction by temperature change above T_g and by physical aging gives rise to enhanced short-range ordering, (b) the volume contraction by temperature change below T_g and the spontaneous volume expansion of pressure-densified sample are accompanied with little change in local structural ordering, and (c) the pressure-densified samples, despite their much higher density, exhibit greatly reduced local ordering. The results suggest that the properties of glassy materials, such as the mechanical relaxation rate, are determined not only by the free volume content but also by the state of local packing of segments. The results also show that an approximate measure of the local structural order can be obtained in practice by measuring the height of the amorphous peak intensity.

I. Introduction

The concept of free volume has been one of the most widely utilized in interpreting phenomena associated with the glass transition and glassy state of polymers. The early work by Fox and Flory[1] and by Simha and Boyer[2] led to the suggestion that the glass transition point could be regarded as an iso-free volume state. The Doolittle equation,[3] giving the relationship between the viscosity and free volume of liquids, has provided a theoretical basis for the WLF equation. The physical aging of glassy polymers, which is manifested as slow increase[4] with time in mechanical moduli accompanied by slow contraction[5] of volume, can be rationalized in terms of the decreasing free volume leading to increased mechanical relaxation time.

The free volume is envisaged as the excess space, unoccupied by molecules, which is dynamically shared by the molecules in their thermal motion. It is usually defined as the difference between the total volume and the "occupied" or "core" volume of the molecules. The latter is often defined differently by different workers. The simplicity and plausibility of the concept underlie its wide acceptance for the interpretation of a variety of physical phenomena. The lack of a precise definition of the occupied volume, however, renders its *quantitative* application difficult. The incorporation of more explicit definition of free volume in recent theories[6,7] remedies this deficiency to some extent, without, however, clarifying its molecular meaning entirely.

Even on a qualitative level, inadequacy of the simple free volume concept has been noted over the years in many instances. For example, specimens of the same glassy polymer, brought to the state of the same density, may exhibit very different properties depending on their prior thermal histories. Such a "memory effect" was described by Kovacs[5] in the volume expansion and contraction following a two-step temperature jump. Similarly, the rate of expansion of volume of pressure-densified glasses after pressure release[8,9] depends on the pressure to which they

0024-9297/87/2220-2723$01.50/0

were subjected to in the past and not simply on the current density. Moreover, reductions in the total volume (hence, presumably, in the free volume) by physical aging and by application of pressure give rise to changes in the mechanical properties in the opposite sense—embrittlement in the former and enhanced ductility[10] in the latter case. These examples illustrate that for a glassy polymer at a given temperature and pressure, the knowledge of its total volume (or free volume) does not guarantee the prediction of its future behavior. In fact, when the Prigogine–Defay ratio[11]

$$\Delta C_p \Delta\beta / TV(\Delta\alpha)^2 \tag{1}$$

is evaluated by use of the observed changes, at T_g, of heat capacity C_p, isothermal compressibility β, and thermal expansion coefficient α, it turns out[11,12] to be different from unity for most glassy polymers. It thus signifies that specification of the free volume, as the order parameter, by itself is not sufficient to describe the nonequilibrium state of the glassy state and that more than one order parameter have to be specified.

A natural extension of the concept of free volume, as a way out of the difficulties mentioned above, is to consider the distribution of free volume. One may rationalize that two specimens of the same glassy polymer, having the same specific volume but different thermal histories, could possess different free volume distributions and thus exhibit different behaviors. A nonuniform distribution of local free volume would manifest itself as a nonuniformity in the local density—i.e., density fluctuation. The concept of a nonuniform local density was incorporated in the theory of polymer conformation relaxation by Robertson,[13] leading to a prediction of isothermal volume relaxation agreeing well with observation. Density fluctuation is, fortunately, a quantity which is amenable to direct experimental measurement by X-ray scattering techniques. A number of such measurements on glassy polymers have already been reported.[14-19]

The quantity, termed density fluctuation $\psi(v)$, that is determined from the X-ray scattering measurement can be defined unambiguously as follows. We consider a reference volume v of a certain size and shape. As this reference volume is moved around in the sample, the number N of particles (electrons or atoms) falling within the volume fluctuates about the mean $\langle N \rangle$. The density fluctuation is defined as the ratio of the variance to the mean

$$\psi(v) = \langle (N - \langle N \rangle)^2 \rangle / \langle N \rangle \tag{2}$$

Defined in this way, $\psi(v)$ is a slowly varying function of the magnitude of v when v is relatively large and converges to a finite value in the limit of $v \to \infty$ (thermodynamic limit). For equilibrium liquids, the density fluctuation in the thermodynamic limit is related to the isothermal compressibility β_T by

$$\psi(\infty) = \rho k T \beta_T \tag{3}$$

where ρ is the average density of the particles. For glasses $\psi(\infty)$ consists of two contributions

$$\psi^{glass} = \psi_{dyn} + \psi_{qst} \tag{4}$$

where the quasi-static contribution ψ_{qst} arises from the part frozen in at T_g and the dynamic contribution ψ_{dyn} is related[20] to the isothermal compressibility $\beta_T{}^g$ of the glass by

$$\psi_{dyn} = \rho k T \beta_T{}^g \tag{5}$$

The intensity $I(\mathbf{q})$ of X-rays scattered in the direction $\mathbf{q}$ ($q = 4\pi \sin\theta/\lambda$) is related to the density fluctuation by

$$\psi(v) = (1/8\pi^3 \rho V) \int I(\mathbf{q})(1/v)[\phi(\mathbf{q})]^2 \, d\mathbf{q} \tag{6}$$

where V is the scattering volume of the sample and $\phi(\mathbf{q})$ is the Fourier transform of the form factor representing the reference volume v. The derivation of eq 6 was first given by Ruland[21] and is also discussed in the Appendix. When $v \to \infty$, $[\phi(\mathbf{q})]^2/v$ becomes a delta function and eq 6 reduces to

$$\psi(\infty) = \lim_{q \to 0} I(q)/\rho V \tag{7}$$

In the reported studies[14-19] of density fluctuation in glassy polymers, only the thermodynamic limit $\psi(\infty)$ was evaluated and discussed. In the present study, we determine $\psi(v)$ for amorphous polystyrene as a function of the size of v. Obviously, a greater amount of information is potentially contained in $\psi(v)$ than in $\psi(\infty)$. To be able to evaluate $\psi(v)$ one needs measurements of $I(q)$ over a range of q values, as is evident from eq 6. We employ a one-dimensional position-sensitive detector to collect $I(q)$ for $q = 0$–16 nm^{-1} in this work, as is described in the Experimental Section. For $I(q)$ at still higher q values, we utilize the wide-angle X-ray data for amorphous polystyrene reported in the literature.[22]

In this work we subject polystyrene samples to five different methods of inducing volume change, and then measure the accompanying changes in the X-ray scattering intensity. The five different methods are as follows: (i) by change in temperature above T_g, (ii) by change in temperature below T_g, (iii) by pressure densification, that is, by applying pressure well above T_g, followed by cooling under the pressure and then releasing the pressure at room temperature, (iv) by allowing spontaneous volume expansion of such pressure densified glasses, and (v) by physical aging, i.e., spontaneous slow contraction of volume on annealing at temperatures below T_g. The volume change induced by temperature change above T_g is accompanied by change in free volume and is thus expected to be different in its effect on the structure of the material than below T_g where volume change presumably proceeds without any change in free volume. The volume contraction produced by pressure densification results in enhanced ductility as opposed to the embrittlement accompanying the volume contraction produced by physical aging, and we seek an explanation for these opposing effects on mechanical properties accompanying volume changes.

Traditionally, the X-ray (or neutron) scattering intensities $I(q)$ from amorphous, single-component material are interpreted in terms of the radial distribution function (or atomic pair correlation function) $g(r)$, which can be derived from $I(q)$ (in the case of monatomic liquids and glasses) by

$$g(r) - 1 = \frac{1}{2\pi^2 \rho} \int i(q) q \frac{\sin qr}{r} \, dq \tag{8}$$

with

$$i(q) = I(q)/Nf^2(q) - 1 \tag{9}$$

where $f(q)$ is the atomic scattering factor and N is the number of atoms in the scattering volume. Both eq 6 and 8 represent integral transformation converting the intensity $I(q)$, a function in reciprocal space, into either $\psi(v)$ or $g(r)$, functions in real space. The information contents that can be obtained from $\psi(v)$ and $g(r)$ are therefore entirely equivalent in principle, especially when $I(q)$ is available for a full range of q: $0 \approx \infty$. (The relationship between $\psi(v)$ and $g(r)$ is discussed in the Appendix.) In practice,

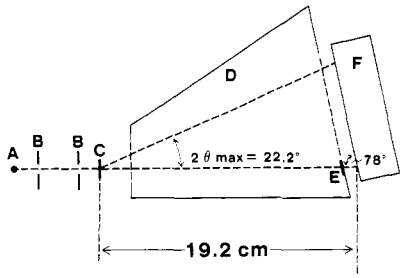

Figure 1. Schematic illustration of the camera geometry: (A) X-ray source, (B) pinhole collimators, (C) sample, (D) vacuum chamber, (E) beam stop, and (F) position-sensitive detector.

however, there are some advantages in evaluating $\psi(v)$ rather than $g(r)$. The kernal (or the weighting factor) in the integral transformation in eq 8 is equal to $(q/r) \sin qr$, which increases in its amplitude with increasing q. Thus, a collection of accurate intensity data $i(q)$ to large q is very important to obtain a reliable radial distribution function. In contrast, in the transformation for $\psi(v)$ given by eq 6, the kernal $[\phi(q)]^2/v$ has a maximum at $q = 0$ and decays to zero at high q, its full width at half maximum being of the order of $1/v$. Thus, the collection of intensity data at high angles becomes much less critical. This difference in the experimental requirement reflects the fact that the radial distribution function is a device to examine the detailed short-range structure in amorphous materials, while the density fluctuation analysis focuses on the packing of atoms on more coarse scales (including the macroscopic scale in the thermodynamic limit $v \rightarrow \infty$).

II. Experimental Section

A. Materials and Sample Preparation. The polymer used in this work is a commercial polystyrene, supplied by Mansanto Co., which was prepared specially to contain no additives. Its viscosity-average molecular weight, determined in cyclohexane solution at 35 °C, is 215 000. This is the same material as used in our previous work.[9,17,19] The polymer pellets were dried under vacuum at about 100 °C overnight before molding into a disk of 1.27-cm diameter and 0.25-cm thickness. The pressure-densified sample was prepared by the same procedure as described earlier[9,19] by means of a hydraulic press. The pressure–temperature cycle employed was briefly as follows. The sample was, at first, heated under atmospheric pressure to a temperature which was estimated to be about 30 °C above the glass transition temperature under the intended pressure. After application of the pressure (between 0.5 and 2.5 kbar), the sample was cooled at 3 deg/min still under the pressure, which was finally released at room temperature.

B. X-ray Measurement. Small-angle scattering data were obtained, as described in our earlier work,[7,19] by use of a Kratky camera, in which the beam length was somewhat reduced to match the sample size. The scattered X-ray intensities in the intermediate angle range (q = 1–16 nm^{-1}) were measured by use of a specially constructed camera in combination with a Tennelec one-dimensional position sensitive detector. The primary beam of Ni-filtered Cu radiation, from a Philips XRG 3100 generator operating at 45 kV and 35 mA, was collimated by means of two pinholes of 0.08-cm diameter separated by 5 cm from each other. The sample was mounted at about 2.5 cm from the second pinhole. This produces a nominal maximum beam divergence of 1.75° and an irradiated area of 0.15 cm diameter at the sample position. The position-sensitive detector, of total effective window length of 8 cm, was mounted at a distance 19.2 cm from the sample position. The detector was inclined from the vertical by 12°, as indicated in Figure 1. In this way, the maximum scattering angle that can be observed was 2θ = 22.2°. A vacuum chamber with thin Mylar windows at both ends was interposed between the sample and the detector to minimize air scattering.

The sample holder was fitted with cartridge heaters and thermocouples to control the temperature. Scattered X-ray intensities were measured at 142, 133, 124, 115, and 104 °C above T_g and at 80, 71, 62, 52, 43, and 34 °C below T_g. The data collection time was 8000 s at each temperature. The highest temperature studied, 142 °C, was dictated by the necessity to keep the sample from sagging by viscous flow during the measurement. The pressure-densified samples, prepared at 0.5, 1.5, and 2.5 kbar, were studied at room temperature immediately after removal from the pressure cell. The intensity measurement commenced 5 min after pressure release and lasted for 2000 s. The intensity change accompanying isothermal volume expansion of pressure-densified samples was studied at 50 °C, the data collection lasting for 3000 s in the initial stage (50 min after the pressure release), and 5000 s in the later stage (5000 min after the pressure release). The shorter data collection time in the early stage was necessitated by the rather appreciable rate of volume expansion. For the physical aging study, the sample, first heated to 120 °C, was quickly brought to the annealing temperature (93 or 85 °C) and the measurement commenced in 5 min. Thereafter, the sample was kept in the X-ray camera at the annealing temperature, and the intensity was collected for 3000 s in the initial stage and for 5000 s in the later stages.

Any possible variations in the primary beam intensity, either due to the generator instability or to subtle changes in the camera alignment, were monitored by means of a scintillation counter mounted to receive some stray radiation from the camera, and also by measuring the intensity scattered by a reference sample at frequent intervals.

C. Data Treatment. A number of corrections were applied to the raw intensity data before they were considered for interpretation. The corrections for the background (air and parasitic scattering), nonuniformity of the detector sensitivity along its length, and the polarization factor were made in the usual manner. In the absorption correction, the effect of increased path lengths through the sample (held perpendicular to the primary beam) at higher scattering angles was taken into account. The camera geometry, utilizing a position-sensitive detector with a straight anode wire, necessitated additional corrections. This is because the 2θ interval subtended by a unit length of the detector anode depends on the position on the wire, and the distance from the irradiated spot on the sample to the detector wire also varies somewhat with 2θ angle. After these corrections, the intensity was scaled to absolute electron units by comparison with low angle data from the same sample. The latter, obtained by use of a Kratky camera, were in turn placed on an absolute scale by means of a calibrated Lupolen standard.[23] Finally, from the intensity data thus obtained, the incoherent (Compton) scattering intensity was subtracted, by utilizing the values of incoherent scattering for hydrogen[24] and carbon[25] available in the literature. Details of the data correction procedures are described elsewhere.[26]

To evaluate the density fluctuation $\psi(v)$, by means of eq 6, as a function of the size of the reference volume v, the intensity $I(q)$ for the whole range of q ($0 \approx \infty$) is required. Because the weighting factor under the integral, $[\phi(q)]^2/v$, decreases rapidly for q values larger than $1/v$, the $I(q)$ data at high q are relatively unimportant. Nevertheless, it is desirable that the $I(q)$ data be available to higher q than the upper limit, 15.6 nm^{-1}, attainable with our camera. We therefore decided to splice our data to the wide-angle X-ray data of amorphous polystyrene available in the literature. There are two such reports,[22,27] in each of which measurements were made at room temperature with a single sample. All our data (in the low and intermediate q range) determined under various conditions were spliced with the single $I(q)$ curve in the high q range reported by Mitchell and Windle.[22] The composite curves thus obtained therefore reflect the effect of temperature and thermal histories of the samples only in the low and intermediate q range. This means that the features we deduce from the composite curves are accurate only to the resolution of about 0.4 ($\sim 2\pi/15$) nm and larger. This does not affect the conclusions we draw in the next two sections, especially since many of our interpretations are derived directly from examination of our $I(q)$ data up to the intermediate q range and do not rely on the composite $I(q)$ curves or their transformations into $\psi(v)$.

Figure 2 plots two of our own data obtained at 25 and 140 °C and the data by Mitchell and Windle.[22] (In this and subsequent figures displaying X-ray intensities, the ordinate gives $I(q)/\rho V$ in electron units per carbon atom, ρ representing the number density of carbon atoms in the sample.) The data by Mitchell and Windle, available only in relative scale in the literature,[22] were

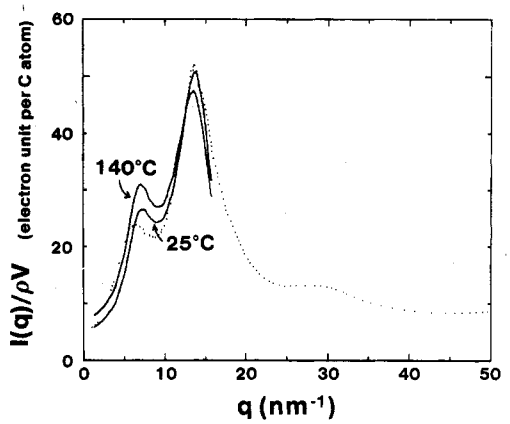

Figure 2. The X-ray intensity data obtained in our work at two temperatures (solid curves) are compared with the result reported by Mitchell and Windle[22] (dotted curve). The ordinate, $I(q)/\rho V$, is in electron units per carbon atom, where V is the scattering volume and ρ is the number density of carbon atoms.

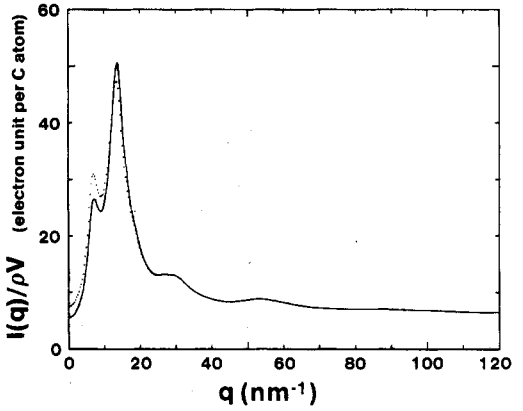

Figure 3. The composite intensity curves obtained by splicing our observed curves ($q < 15$ nm^{-1}) with the data by Mitchell and Windle[22] ($q > 15$ nm^{-1}) by the method described in the text: solid curve, 25 °C; dotted curve, 140 °C.

rescaled by us to absolute units by means of the method described by Krogh-Moe.[28] In order to achieve a smooth transition from our data ($q < 15$ nm^{-1}) to the data by Mitchell and Windle ($q > 15$ nm^{-1}), the latter were multiplied by an arbitrary scaling function $y(q) = 1 - A \exp(-Bq^2)$. The two adjustable parameters A and B were assigned values to satisfy the following two criteria. (i) After multiplication by $y(q)$, the intensity value of Mitchell and Windle becomes equal to our measured value at $q = 15$ nm^{-1}. (ii) $y(q)$ differs from unity by not more than 0.01 for q beyond 24.5 nm^{-1}. This second criterion forces all the composite curves for samples under different conditions to have the same $I(q)$ curves at q values beyond 24.5 nm^{-1}. Examples of the composite curves obtained by splicing our low-angle and intermediate-angle data with those of Mitchell and Windle are shown in Figure 3.

III. Results

The scattered intensities were determined at five temperatures (142, 133, 124, 115, 104 °C) above T_g and at six temperatures (80, 71, 62, 52, 43, 34 °C) below T_g. Some of the curves are plotted in Figures 4 and 5. (In these and subsequent plots of $I(q)$, unless otherwise stated, the incoherent scattering intensities have not been subtracted, and the ordinate gives the intensity in electron units per carbon atom.) The peak at $q = 13.8$ nm^{-1} is the so-called amorphous halo, observable with all noncrystalline materials. The peak at $q = 7.5$ nm^{-1} has been termed "polymerization ring" in the early work of Katz.[29] A similar secondary peak at lower q than the main amorphous peak has been observed with a number of amorphous polymers,[30] and attempts have been made to identify it with some specific local ordering of the polymer chains involved.

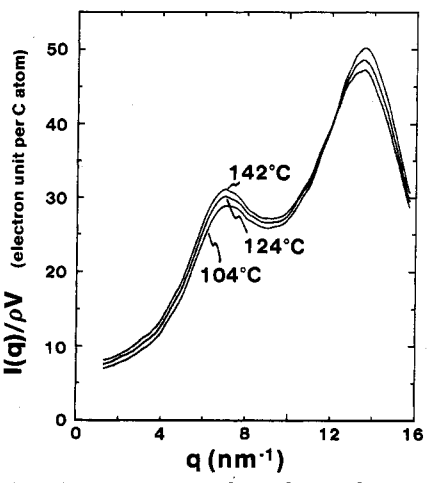

Figure 4. The X-ray intensity data observed at 142, 124, and 104 °C, all above T_g. The ordinate is the scattered intensity in electron units per carbon atom, and the intensity includes the incoherent scattering.

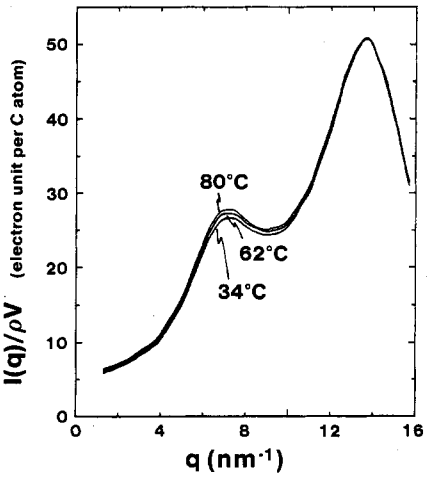

Figure 5. The X-ray intensity data observed at 80, 62, and 34 °C, all below T_g. Note that the intensity around the amorphous peak does not change with temperature.

In this work, however, we are not concerned with identification of the structural elements that give rise to these peaks. Rather, we note, by comparing Figures 4 and 5 that with a decrease in temperature the intensities below q = ca. 11 nm^{-1} decrease fairly uniformly, in both the liquid and glassy states, while the pronounced increase in the height of the amorphous peak for the liquid is not matched by the glass. Although the temperature intervals covered below and above T_g are comparable, the overall magnitude of the change observed in the glassy state is much smaller, and this reflects the smaller volume change occurring with the glassy material. A better comparison is to examine the changes in X-ray intensity accompanying comparable changes in volume. Such a comparison is shown in Figures 6 and 7 for the temperature changes, 140–118 °C above T_g and 80–25 °C below T_g, which lead to the same magnitude of volume decrease, $\Delta v_{sp} = 0.0113$ cm^3/g. These curves were constructed by fitting a linear regression line, at each q, to the intensities observed at various temperatures (either above or below T_g), and then by interpolation or extrapolation. These two figures show that the changes in the intensity curves brought about by the same amount of volume contraction are entirely comparable in the q range below about 11 nm^{-1}, but there is a clear difference around the amorphous halo, depending on whether the material is in the liquid or glassy state. When the intensity of the subsidiary peak at $q = 7.8$ nm^{-1} is plotted against

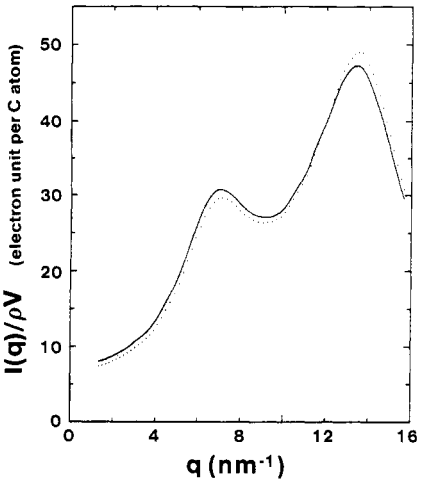

Figure 6. X-ray intensities at 140 (solid curve) and 118 °C (dotted curve), calculated by interpolation of the data obtained at five temperatures: 142, 133, 124, 115, and 104 °C. The two temperatures shown are chosen so as to represent a change in specific volume by 0.0113 cm^3/g.

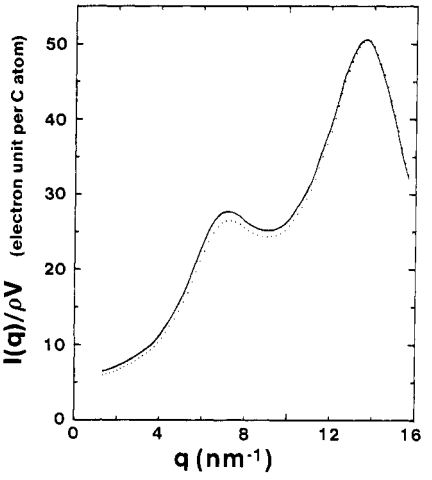

Figure 7. X-ray intensities at 80 (solid curve) and 25 °C (dotted curve), the latter calculated by extrapolation of the data obtained at 80, 71, 62, 52, 43, and 34 °C. The difference in the specific volume of polystyrene between 25 and 80 °C is equal to 0.0113 cm^3/g.

the specific volume, the data both below and above T_g fall together on a single straight line, indicating that the intensity is determined uniquely by the specific volume, irrespective of whether the material is in the liquid or glassy state. This means that as far as large-scale density fluctuation or long-range ordering are concerned, there are no essential differences between the liquid and glass. The structural difference between these two states of the material has to be found in features revealed by intensities at q higher than 11 nm^{-1}, that is, in their short-range structure of around 0.5-nm distance scale or smaller.

The effect of volume densification under pressure, achieved by application of pressure above T_g and subsequent pressure release at room temperature, was studied with samples prepared at 0.5, 1.5, and 2.5 kbar. The intensity data obtained with the samples prepared under atmospheric pressure and under 2.5 kbar are compared in Figure 8. The data for the other two samples fall appropriately between these two curves. The volume contraction achieved by the 2.5 kbar pressure is equal to 0.0113 cm^3/g. The difference between the two curves in the q range below 11 nm^{-1} is almost identical with those found in Figures 6 and 7. The features above 11 nm^{-1} in q are different yet from either of those shown in Figures

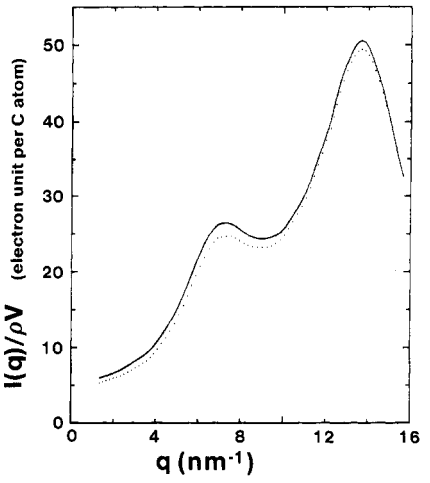

Figure 8. The scattered X-ray intensity observed at 25 °C with a sample prepared under 2.5 kbar (by applying the pressure above T_g and releasing the pressure at room temperature) (dotted curve) is compared with the intensity observed with an ordinary polystyrene sample prepared under atmospheric pressure (solid curve). The specific volume of the pressure-densified sample is smaller than the latter by 0.0113 cm^3/g.

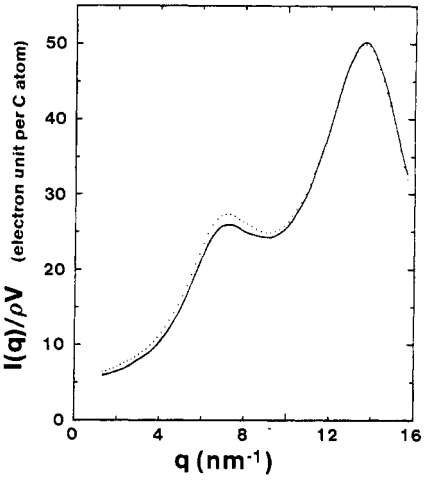

Figure 9. The curves illustrate the changes in X-ray intensities scattered from a pressure-densified sample (prepared under 2 kbar) undergoing spontaneous volume expansion when annealed at 50 °C. The solid curve was observed at 50 min of annealing, and the dotted curve was obtained by extrapolation of the curve observed at 5000 min of annealing, so that the volume change between these two curves corresponds to 0.0113 cm^3/g.

6 and 7: the height of the amorphous peak is reduced when the volume is compressed by pressure, whereas the height is enhanced when the volume is reduced by temperature decrease in the liquid state.

The changes accompanying the spontaneous volume expansion of pressure-densified samples were studied with two samples, prepared under 1 and 2 kbar. The samples, after pressure release at room temperature, were immediately transferred to the camera sample holder, maintained at 50 °C, and the scattered intensities were determined at 50 and 5000 min after the sample was taken out of the pressure mold. (Because of the very rapid expansion of volume immediately after pressure release, meaningful measurements could not be made before 50 min.) The total volume expansion occurring during this time interval was 0.0017 and 0.0040 cm^3/g for the 1 and 2 kbar samples, respectively. The change in the intensity curves observed was correspondingly fairly small. In order to facilitate comparison with results given in Figures 6–8, in Figure 9 we plot curves which were "normalized" to a volume expansion of 0.0113 cm^3/g. In other words, the changes in

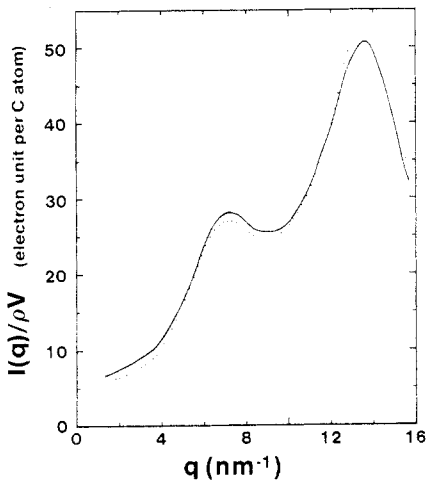

Figure 10. The curves show the changes in X-ray intensities scattered from a sample undergoing isothermal annealing (physical aging) at 93 °C. The solid curve was observed at 50 min of annealing, and the dotted curve was obtained by extrapolation of the curve observed at 5000 min, so that the volume change between the two curves shown corresponds to 0.0113 cm^3/g.

the scattering curve observed at the end of 5000 min with the 2 kbar sample was accentuated by a factor 0.0113/0.0040. Again, the magnitudes of the changes shown in Figure 9 for q less than 11 nm^{-1} are comparable to those shown in Figures 6–8. The change in intensity around the amorphous peak is very small and resembles most closely the results given in Figure 7 which pertain to a volume change induced by temperature change in the glassy state.

Finally, we present the results obtained with the sample undergoing physical aging, that is, when the polystyrene sample, prepared in the ordinary manner under atmospheric pressure, was annealed isothermally at a temperature below T_g. X-ray intensity measurements were made at 50 and 20 000 min of annealing at 84 °C and at 50 and 5000 min of annealing at 93 °C. The decrease in volume realized in these time intervals was 0.0014 cm^3/g at 84 °C and 0.0010 cm^3/g at 93 °C. In Figure 10 we again plot not the intensity curve actually observed but rather the "normalized" curve which corresponds to a volume change of 0.0113 cm^3/g. It shows that the height of the amorphous peak has been enhanced markedly as a result of physical aging. The structural change accompanying physical aging therefore resembles the one occurring on reduction of volume upon cooling above T_g. Evidently, physical aging leads to a more highly ordered structure in the same sense that the equilibrium liquid structure is more ordered at lower temperature. Comparison of Figure 10 with Figure 9 shows that the isothermal volume expansion of pressure-densified samples and the isothermal volume contraction of samples undergoing physical aging differ not only in the direction of the volume change but also in some fundamental way in the nature of the structural rearrangements which underlie such volume expansion or contraction.

Instead of examining the intensity curves directly, as discussed above, we now transform the $I(q)$ data first into density fluctuation $\psi(v)$ by means of eq 6. For this purpose we need $I(q)$ curves extending to higher q values and therefore augment our observed $I(q)$ curves by splicing them to the wide-angle X-ray data reported by Mitchell and Windle,[22] as described in the Experimental Section. In performing the transformation indicated by eq 6, $\phi(q)$ was given the explicit expression, eq A16 in the Appendix, which is applicable to a sphere of diameter D. In addition, the composite intensity $I(q)$ was divided by $f_C^2 + f_H^2$ (f_C and f_H being the atomic scattering factors of carbon and

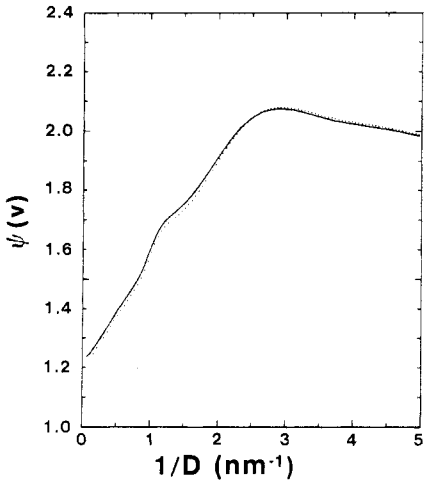

Figure 11. The observed intensity $I(q)$, spliced together with the high angle data ($q > 15$ nm^{-1}) of Mitchell and Windle,[22] were transformed into the density fluctuation $\psi(v)$ by means of eq 6. The reference volume v is assumed to be a sphere of diameter D, and for the Fourier transform $\phi(q)$ of its form factor eq A16 was used. The two curves shown for 140 (solid curve) and 118 °C (dotted curve), both above T_g, were calculated from the intensity data shown in Figure 6. The value at the abscissa $1/D$ equal to 0 corresponds to the density fluctuation in the thermodynamic limit. The density fluctuation at shorter size scale increases and reaches a maximum at $D \approx 0.4$ nm, which corresponds roughly to the average nonbonded interatomic distance.

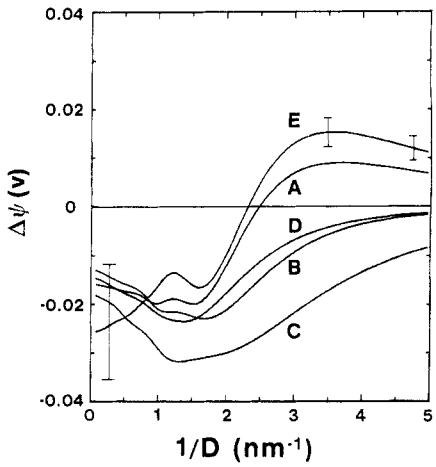

Figure 12. The changes in density fluctuation accompanying a volume decrease of 0.0113 cm^3/g effected by five different methods: (A) temperature change above T_g, (B) temperature change below T_g, (C) pressure densification, (D) isothermal annealing at 50 °C of a pressure-densified sample, and (E) isothermal annealing (physical aging) of an ordinary sample at 93 °C. The error bars are given for the worst case, physical aging, in which the total volume change actually observed was the smallest. For large-scale density fluctuation, i.e., for D greater than about 0.5 nm, no qualitative difference can be found among the five curves. The greatest differences are observed for small-scale density fluctuation, i.e., for D between about 0.3 and 0.4 nm, where the change accompanying volume decrease is positive (enhanced short-range ordering) for curves A and E, while negative for the other three cases.

hydrogen atoms, respectively) before they were subjected to the integration indicated by eq 6. The $\psi(v)$ function thus obtained therefore represents the fluctuation of the density of C–H pair rather than the electronic density fluctuation. Figure 11 shows two $\psi(v)$ curves which were derived from the two $I(q)$ curves shown in Figure 6 that pertain to 140 and 118 °C, respectively. The differences between the two $\psi(v)$ curves are rather small, but we can magnify the differences by plotting $\Delta\psi(v)$ against $1/D$. Such plots are given in Figure 12, where each curve shows

$\Delta\psi(v)$ resulting from volume contraction of $\Delta v_{sp} = 0.0113$ cm^3/g induced by one of the five methods described before. To indicate that sufficient precision exists even for these $\Delta\psi(v)$ curves, error bars, based on the estimation of the errors in observed $I(q)$ data and their propagation through the transformation, are given for curve E (changes induced by physical aging), which represents the *worst* case in view of the very small total volume change actually observed.

In Figure 12, the large-scale density fluctuations $\psi(v)$ corresponding to $D >$ ca. 0.5 nm all show qualitatively the same trend as the volume reduction is induced by different means. It means that the large-scale density fluctuation, including the thermodynamic limit $\psi(\infty)$, is determined primarily by specific volume and is largely independent of prior thermal histories. The differences among the five curves are most evident for D in the range 0.25–0.4 nm. The small-scale density fluctuation for D on the order of interatomic distances can be interpreted, in general, as an indicator of the structural order of the corresponding size scale. For example, a highly ordered, crystalline structure will give very high values of density fluctuation function for D matching the lattice repeat distances. In Figure 12, a positive $\Delta\psi(v)$ in the range of D = 0.25–0.4 nm means that the short-range order of segmental packing is enhanced when the specific volume is reduced. Of the five curves in Figure 12, two of the curves, A and E, show positive $\Delta\psi(v)$ and three, B, C, and D, show negative $\Delta\psi(v)$ in this range of D. Thus, when the volume is reduced either by lowering the temperature in the liquid state or by physical aging, a better short-range ordering is realized. Such improved packing of neighboring segments undoubtedly leads to a reduced segmental mobility which one normally associates with a reduction in free volume. When the specific volume is altered by temperature change in the glassy state or by volume relaxation of pressure-densified glasses, the volume change is accompanied with very little change in the local ordering. On pressure densification, the reduced specific volume is accompanied by a reduced, and not enhanced, short-range ordering. If the increased local ordering induced by physical aging results in reduced segmental motion and thus to loss of ductility, it is then natural to expect the reduced local ordering resulting from pressure densification to produce an enhanced segmental mobility and enhanced ductility. This is in accord with experimental observation. We might even say that the reduction in specific volume resulting from pressure densification actually leads to an increased free volume, if we interpret the term "free volume" liberally and use it to mean a measure of segmental mobility and not a simple measure of unoccupied volume. The local structure of glasses reflects the structure that was prevailing at the time of the glass formation. With increasing pressure, the temperature of glass transition increases while the specific volume at the glass transition point decreases. The former tends to decrease the local ordering and the latter favors an increase in the local ordering. The fact that increased pressure densification results in reduced local ordering means that the glass transition temperature is more important than the glass transition volume in determining the state of the local order in the resulting glass.

IV. Discussion

The results presented above show that, when volume changes are induced on polystyrene by five different methods, the resulting changes in the density fluctuation on large size scales (including the thermodynamic limit) correlate fairly well with the specific volume, while on much smaller scales (that is, in the range 0.25–0.4 nm, which is comparable to the nonbonded distances between neighboring atoms) the changes in the density fluctuation depend sensitively on the method by which the volume change was effected. This reaffirms the fact that the specification of specific volume alone is not sufficient to characterize the state of a glassy material. The results suggest, furthermore, that the specific volume by itself may not be a good indicator of the mechanical properties of the material, and instead the small scale density fluctuation (or the state of local segmental packing) more faithfully reflects the changes in the mechanical properties resulting from physical aging or pressure densification. Although the small-scale density fluctuation was determined in this work from analysis of the composite $I(q)$ curves extending over the whole q range, an approximate measure could be obtained in practice by simply measuring the height of the main amorphous peak at q around 14 nm^{-1}. The validity of such a simplified procedure can be seen from the fact that essentially the same qualitative conclusions were drawn from Figures 6–10 as from Figure 12.

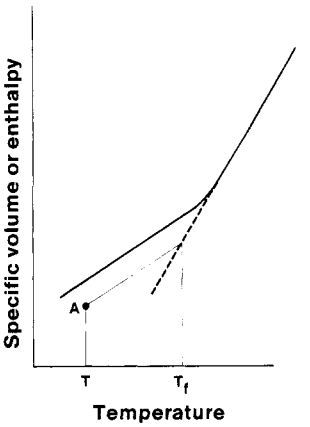

Figure 13. Schematic diagram to illustrate the definition of fictive temperature based on specific volume or enthalpy: heavy solid line, specific volume (or enthalpy) attained on cooling at some fixed cooling rate; heavy broken line, extrapolation of the liquid line down below T_g; A, the state at T of a specimen attained by some specific thermal history (for example, by physical aging or compression); T_f, the fictive temperature of the specimen represented by point A. For an equilibrium liquid T_f and T coincide, but for glasses T_f is always higher than T, implying that the internal structure of the glassy specimen corresponds to the structure of the equilibrium liquid at T_f.

The fictive temperature T_f, originally proposed by Tool,[31] has been utilized as a means of specifying the state of a glassy sample. The fictive temperature, defined as illustrated in Figure 13, allows for the fact that the volume change occurring on cooling below T_g is mostly "elastic" and involves no change in the free volume. Such fictive temperature can be defined either with respect to volume or with respect to enthalpy, and these two fictive temperatures appear to agree well with each other in most cases. We may also define a fictive temperature on the basis of the type of short-range ordering that is discussed in this work. That is, a glassy sample can be said to have a value $T_{f\psi}$ of the structural fictive temperature if the height of the amorphous peak observed is the same as that exhibited by the same material in an equilibrium state at temperature $T_{f\psi}$. Defined this way, the structural fictive temperature will change little as the sample is cooled below T_g under atmospheric pressure, just as the volumetric or enthalpic fictive temperature would remain constant. These three types of fictive temperatures considered here probably agree with each other well also when the state of the sample is altered by physical aging. However, when the glass sample is subject to high pressure or some com-

plex thermal histories, the fictive temperatures based on volume and on the short-range structural order are likely to diverge from each other. Our results in this work show, for example, that for pressure-densified samples the fictive temperature $T_{f\psi}$ based on the short-range structure is considerably higher than the fictive temperature T_{fv} based on specific volume. Characterization of such a sample then requires the explicit specification of both of these fictive temperatures.

The irreversible thermodynamics based on the concept of order parameters has, despite its elegant formalism, found only a modest utility so far, and this is in part due to the difficulty of identifying the order parameters with any concrete molecular features. The specific volume, which deviates from its equilibrium value below T_g, can obviously be used as one of the order parameters. The empirical fact that the Prigogine–Defay ratio deviates from unity dictates, however, that more than one order parameter is specified. We may therefore propose that the fictive temperature $T_{f\psi}$ or some similar measure of the short-range order such as the height of the amorphous peak be utilized as the second order parameter. Whether these two order parameters would suffice to describe the behaviors of glassy materials completely remains to be seen, but the use of these two would certainly give a much better description of the thermodynamic state of a glassy material than the specific volume alone can.

An interesting question, which remains to be answered, is: "Which of the two factors, the specific volume or the local structural order, is more important in determining the properties of glassy materials, such as the rate of mechanical relaxation?". There is some evidence indicating that the degree of local structural order is more important. For example, it has long been known that a sample, aged physically and thus rendered brittle, can be brought to the original ductility (i.e., "rejuvenated") by application of a moderate tensile stress. This had been explained by saying that the dilatational stress induced by elongation restores the specific volume to the original state before the physical aging. However, recent studies show that such rejuvenation can be achieved by torsional or even compressional deformation,[32,33] neither of which produces dilatational effect. It is more likely that the effect of deformation, irrespective of whether tensile, torsional or compressive, disrupts the local packing of segments from their low-energy state achieved by the physical aging and elevates it to a more disordered state of higher energy. Another indication of the importance of the degree of local segmental packing in determining the properties of glasses is seen in DSC study of pressure-densified materials. The DSC thermograms,[34,35] obtained on heating such materials, show a minor, yet clearly recognizable, peak at temperatures some 30–50 deg below the normal T_g. The peak evidently arises from some structural reorganization triggered while apparently still in the glassy state. Such unusually enhanced segmental mobility probably arises from the presence of a relatively high degree of disorder in the local segmental packing that was built in at the time of vitrification under high pressure. One may even regard the low-temperature peak in the thermogram as indicating an onset of glass–rubber transition in the densified sample. The transition is, however, aborted prematurely when a slightly higher temperature is reached, since then the rate of relaxation is again reduced as the disordered local segmental packing reverts to more stable configurations, while the accompanying volume expansion is not rapid enough to counteract it. The notion that a higher density sample can have a much lower glass transition temperature can be rationalized easily if we accept that the glass transition temperature might be determined not only by the density but also by the degree of local ordering. The glass transition point is then to be regarded not as an iso-free-volume state but as a state of iso-relaxation time dictated by the combination of free volume and the degree of short-range structural ordering. Indeed, such a view could more readily be reconciled with the other commonly subscribed view of regarding the glass transition point as an iso-entropic state.

Acknowledgment. This work was supported in part by NSF Grants DMR83-00760 and 85-20921.

Appendix. Density Fluctuation and Spatial Correlation of Density Fluctuation

Here we give the derivation of the equations enabling the evaluation of density fluctuation $\psi(v)$ and the spatial correlation $\psi_R(v_1,v_2)$ of density fluctuation from X-ray intensity $I(q)$. We also discuss the relationship between these density fluctuation functions and the pair correlation function $g(r)$.

Extending the concept of density fluctuation defined by eq 2, one can consider the spatial correlation of density fluctuation as follows. Consider a reference volume v_1 (of arbitrary shape and size) placed at $\mathbf{r}$ and another reference volume v_2 (possibly of different shape and size) placed at $\mathbf{r} + \mathbf{R}$. Let N_1 and N_2 be the number of particles (electrons or atoms) falling within v_1 and v_2, respectively. The correlation $\psi_R(v_1,v_2)$ of density fluctuation is then defined by

$$\psi_R(v_1,v_2) = \frac{\langle (N_1 - \langle N_1 \rangle)(N_2 - \langle N_2 \rangle) \rangle}{\langle N_1 \rangle^{1/2} \langle N_2 \rangle^{1/2}} \tag{A1}$$

where the brackets denote the average over all values of $\mathbf{r}$ within the sample. The density fluctuation $\psi(v)$ considered in eq 2 then amounts to a self-correlation: $\psi_0(v,v)$.

Now we define a function $\eta(\mathbf{r}) \equiv \rho(\mathbf{r}) - \langle \rho \rangle$, where $\rho(\mathbf{r})$ is the density of the particles at position $\mathbf{r}$. We also define the form factor $v_1(\mathbf{r})$ of the reference volume v_1 such that $v_1(\mathbf{r}) = 1$ if $\mathbf{r}$ is within the volume and $= 0$ if it is outside it. The deviation of the number N_1 of particles within the volume v_1 from its average $\langle N_1 \rangle$ can then be written as

$$\delta N_1(\mathbf{r}) = \gamma_1(\mathbf{r}) \tag{A2}$$

where

$$\gamma_1(\mathbf{r}) = \eta(\mathbf{r}) * v_1(\mathbf{r}) \tag{A3}$$

the symbol * denoting a convolution product. To calculate $\psi_R(v_1,v_2)$ we need to evaluate the integral

$$\langle \delta N_1, \delta N_2 \rangle_R = (1/V) \int \gamma_1(\mathbf{r}) \gamma_2(\mathbf{r} + \mathbf{R})\, d\mathbf{r} \tag{A4}$$

where V is the volume of the sample. By use of the Parseval's theorem (or the power theorem, as it is sometimes referred to[36]), we obtain

$$\langle \delta N_1, \delta N_2 \rangle_R = \frac{1}{V(2\pi)^3} \int F\{\gamma_1(\mathbf{r})\} F^*\{\gamma_2(\mathbf{r} + \mathbf{R})\}\, d\mathbf{q} \tag{A5}$$

where $F\{\ \}$ denotes the Fourier transform and $F^*\{\ \}$ its complex conjugate. Application of the convolution theorem then leads to

$$\langle \delta N_1, \delta N_2 \rangle_R = \frac{1}{V(2\pi)^3} \int e^{-i\mathbf{q}\mathbf{R}} |F\{\eta(\mathbf{r})\}|^2 \phi_1(\mathbf{q}) \phi_2^*(\mathbf{q})\, d\mathbf{q} \tag{A6}$$

where $\phi_1(\mathbf{q})$ is the Fourier transform of the form factor $v_1(\mathbf{r})$.

If the particles of interest under consideration are electrons, then $F\{\eta(\mathbf{r})\}$ is related to the intensity $I(\mathbf{q})$ (in

electron unit) of the X-rays scattered in the direction $\mathbf{q}$ by

$$I(\mathbf{q}) = |F\{\eta(\mathbf{r})\}|^2 \quad \text{(A7)}$$

The spatial correlation of the density fluctuation is then given by

$$\psi_{\mathbf{R}}(v_1,v_2) = \frac{1}{(2\pi)^3\rho V}\int e^{-i\mathbf{qr}} I(\mathbf{q})\frac{\phi_1(\mathbf{q})}{v_1^{1/2}}\frac{\phi_2^*(\mathbf{q})}{v_2^{1/2}}\,d\mathbf{q} \quad \text{(A8)}$$

where v_1 is the volume of the form factor $v_1(\mathbf{r})$. When $\mathbf{R} = 0$ and $v_1(\mathbf{r}) = v_2(\mathbf{r}) \equiv v(\mathbf{r})$, eq A8 reduces to eq 6 for $\psi(v)$. If the particles of interest are atoms and the sample contains only one kind of atom, then instead of eq A7 we have

$$I(\mathbf{q})/f^2(q) = |F\{\eta(\mathbf{r})\}|^2 \quad \text{(A9)}$$

where $f(q)$ is the atomic scattering factor. Equations A8 and 6 are correspondingly modified by a factor $1/f^2(q)$.

We now examine the relationship of these density fluctuation functions to the atomic pair correlation function $g(r)$. By defining the interference (or the reduced intensity) function $i(\mathbf{q})$ by

$$i(\mathbf{q}) = I(\mathbf{q})/Nf^2(q) - 1 \quad \text{(A10)}$$

where $N = \rho V$ is the total number of atoms in the sample, eq A6 can be written as

$$\langle\delta N_1,\delta N_2\rangle_{\mathbf{R}} = \frac{\rho}{(2\pi)^3}\int e^{-i\mathbf{qR}}\, i(\mathbf{q})\phi_1(\mathbf{q})\phi_2^*(\mathbf{q})\,d\mathbf{q} + \frac{\rho}{(2\pi)^3}\int e^{-i\mathbf{qR}}\phi_1(\mathbf{q})\phi_2^*(\mathbf{q})\,d\mathbf{q} \quad \text{(A11)}$$

The interference function $i(\mathbf{q})$ is known[37] to be related to the total correlation function

$$h(\mathbf{r}) \equiv g(\mathbf{r}) - 1$$

by

$$i(\mathbf{q}) = \rho\int h(\mathbf{r})e^{-i\mathbf{qr}}\,d\mathbf{r} \quad \text{(A12)}$$

Therefore, by use of the convolution theorem, eq A11 can be recast to

$$\langle\delta N_1,\delta N_2\rangle_{\mathbf{R}} = \rho[\rho h(\mathbf{R})*v_1(\mathbf{R})*v_2(\mathbf{R})] + \rho[v_1(\mathbf{R})*v_2(\mathbf{R})] \quad \text{(A13)}$$

The spatial correlation of density fluctuation then becomes

$$\psi_{\mathbf{R}}(v_1,v_2) = [\rho h(\mathbf{R})*v_1(\mathbf{R})*v_2(\mathbf{R})]/v_1^{1/2}v_2^{1/2} + [v_1(\mathbf{R})*v_2(\mathbf{R})]/v_1^{1/2}v_2^{1/2} \quad \text{(A14)}$$

Equations having the same physical meaning as above, but expressed in very different notations, were previously given by Fisher and Adamovich.[38]

In the limit of $v_1,v_2 \to 0$, eq A14 reduces to

$$\psi_{\mathbf{R}}(0,0) = \rho h(\mathbf{R}) + 1 = \rho[g(\mathbf{R}) - 1] + 1 \quad \text{(A15)}$$

thus indicating the relationship between the density fluctuation correlation and the pair correlation function. The density fluctuation correlation function may therefore be considered as a way of looking at the pair correlation on a more coarse scale or with a reduced resolution where the degree of resolution is equal to the reference volume size v.

If we take a sphere of diameter D as the reference volume v, the Fourier transform of its form factor is given by

$$\phi(q) = 24v[\sin(Dq/2) - (Dq/2)\cos(Dq/2)]/(Dq)^3 \quad \text{(A16)}$$

For an isotropic sample, the correlation of electron density fluctuation between two spherical volume elements, both of diameter D and separated by distance R, then takes the form

$$\psi_{\mathbf{R}}(D) = \frac{48D}{\pi}\int_0^\infty \frac{I(\mathbf{q})}{\rho V}\frac{\sin(qR)}{qR}\times\frac{[\sin(Dq/2) - (Dq/2)\cos(Dq/2)]^2}{(Dq)^4}\,dq \quad \text{(A17)}$$

An equation corresponding to (A17) but applicable only for the case of $R = D$ was previously given by Chay and Frank.[39]

The relationship between $h(R)$ and the density fluctuation $\psi(v)$ can be seen by setting $R = 0$ and $v_1 = v_2 = v$ in eq A14. If we adopt the notation $u(\mathbf{R})$ for the normalized self-convolution of $v(\mathbf{R})$ defined by

$$u(\mathbf{R}) \equiv (1/v)v(\mathbf{R})*v(\mathbf{R}) \quad \text{(A18)}$$

one obtains

$$\psi(v) = 1 + \rho\int h(\mathbf{r})u(-\mathbf{r})\,d\mathbf{r} \quad \text{(A19)}$$

The function $u(\mathbf{R})$ has a maximum value equal to unity at $R = 0$ and decreases monotonically toward zero, which is reached when R is equal to the maximum linear dimension of v (in the direction of $\mathbf{R}$). For example, when v is a sphere of dimater D, $u(\mathbf{R})$ is given by

$$u(\mathbf{R}) = (1 - R/D)^2(1 + R/2D) \quad \text{(A20)}$$

Equation A19 therefore shows that $\psi(v) - 1$ is equal to the weighted integral of $\rho h(\mathbf{r})$, with the range of integration equal to the dimension of v. In the thermodynamic limit, $v \to \infty$, one obtains[37]

$$\psi(\infty) = 1 + \rho\int h(\mathbf{r})\,d\mathbf{r} = \rho kT\beta_T \quad \text{(A21)}$$

Registry No. Polystyrene, 9003-53-6.

References and Notes

(1) Fox, T. G.; Flory, P. J. *J. Appl. Phys.* **1950**, *21*, 581; *J. Polym. Sci.* **1954**, *14*, 315.
(2) Simha, R.; Boyer, R. F. *J. Chem. Phys.* **1962**, *37*, 1003.
(3) Doolittle, A. K. *J. Appl. Phys.* **1951**, *22*, 1471.
(4) Struik, L. C. E. *Physical Aging in Amorphous Polymers and Other Materials*; Elsevier: New York, 1978.
(5) Kovacs, A. J. *Fortschr. Hochpolym.-Forsch.* **1964**, *3*, 394.
(6) Simha, R. *Ann. N. Y. Acad. Sci.* **1976**, *279*, 2 and earlier papers referenced in it.
(7) Cohen, M. H.; Grest, G. S. *Phys. Rev., B. Condens. Matter.* **1979**, *B20*, 1077.
(8) Oels, H. J.; Rehage, G. *Macromolecules* **1977**, *10*, 1036.
(9) Roe, R. J.; Song, H. H. *Macromolecules* **1985**, *18*, 1603.
(10) Yourtee, J. B.; Cooper, S. L. *J. Appl. Polym. Sci.* **1974**, *18*, 897.
(11) Davies, R. O.; Jones, G. O. *Adv. Phys.* **1953**, *2*, 370.
(12) Roe, R. J.; Tonelli, A. E. *Macromolecules* **1978**, *11*, 114.
(13) Robertson, R. E. *J. Polym. Sci., Polym. Phys. Ed.* **1979**, *17*, 597.
(14) Wendorff, J. H.; Fischer, E. W. *Kolloid Z. Z. Polym.* **1973**, *251*, 876, 884.
(15) Rathje, J.; Ruland, W. *Colloid Polym. Sci.* **1976**, *254*, 358.
(16) Wiegand, W.; Ruland, W. *Prog. Colloid Polym. Sci.* **1979**, *66*, 355.
(17) Roe, R. J.; Curro, J. J. *Macromolecules* **1983**, *16*, 428.
(18) Curro, J. J.; Roe, R. J. *Polymer* **1984**, *25*, 1424.
(19) Curro, J. J.; Roe, R. J. *J. Polym. Sci., Polym. Phys. Ed.* **1983**, *21*, 1785.
(20) Roe, R. J. *J. Chem. Phys.* **1983**, *79*, 936.
(21) Ruland, W. *Prog. Colloid Polym. Sci.* **1975**, *57*, 192.
(22) Mitchell, G. R.; Windle, A. H. *Polymer* **1984**, *25*, 906.
(23) Kratky, O.; Pilz, I.; Schmitz, P. J. *J. Colloid Interface Sci.* **1966**, *21*, 24.
(24) Compton, A. H.; Allison, S. K. *X-rays in Theory and Experiment*; Van Nostrand: New York, 1935.
(25) Keating, D. T.; Vineyard, G. H. *Acta Crystallogr.* **1956**, *9*, 895.
(26) Song, H. H. Ph.D. Dissertation, University of Cincinnati, 1986.
(27) Wecker, S. M.; Davidson, T.; Cohen, J. B. *J. Mat. Sci.* **1972**, *7*, 1249.
(28) Krogh-Moe, J. *Acta Crystallogr.* **1956**, *9*, 951.

(29) Katz, J. R. *Trans. Faraday Soc.* **1936**, *32*, 77.
(30) Miller, R. L.; Boyer, R. F.; Heijboer, J. *J. Polym. Sci., Polym. Phys. Ed.* **1984**, *22*, 2021.
(31) Tool, A. Q.; Eichlin, C. G. *J. Am. Ceramic Soc.* **1931**, *14*, 276.
(32) Ricco, T.; Smith, T. L. *Polymer* **1985**, *26*, 1979.
(33) Smith, T. L.; Ricco, T.; Levista, G.; Moonan, W. K. *Plast. Rubber Process. Appl.* **1986**, *6*, 81.
(34) Weitz, A.; Wunderlich, B. *J. Polym. Sci., Polym. Phys. Ed.* **1974**, *12*, 2473.
(35) Prest, W. M., Jr.; Roberts, F. J., Jr. *Ann. N. Y. Acad. Sci.* **1981**, *371*, 67.
(36) Bracewell, R. N. *The Fourier Transform and Its Applications*, 2nd ed.; McGraw-Hill: New York, 1978; p 113.
(37) Kohler, F. *The Liquid State*; Verlag Chemie: Weinheim, Germany, 1972; Chapter 4.
(38) Fisher, I. Z.; Adamovich, V. I. *J. Struct. Chem. USSR (Engl. Transl.)* **1963**, *4*, 759.
(39) Chay, T. R.; Frank, H. S. *J. Chem. Phys.* **1972**, *57*, 2910.

A Surface Light Scattering Study of Poly(ethylene oxide) and Poly(vinyl acetate) at the Air/Water and Heptane/Water Interfaces

Bryan B. Sauer, Masami Kawaguchi,† and Hyuk Yu*

Department of Chemistry, University of Wisconsin, Madison, Wisconsin 53706.
Received April 2, 1987

ABSTRACT: Spread films of poly(ethylene oxide) (PEO) and poly(vinyl acetate) (PVAc) were studied at the interfaces of air/water (A/W) and heptane/water (O/W) by using the Wilhelmy plate method for static surface tension measurements and the surface quasi-elastic light scattering (SLS) method for deducing the dynamic surface viscoelastic parameters. Upon effecting precise measurements at A/W, we show that the surface dilational elasticity determined from the Wilhelmy plate method and the longitudinal elasticity deduced from SLS were the same for a wide surface concentration range. The surface longitudinal viscosity of PEO films was shown to be less than that of PVAc films by a factor of 10 or more. To our knowledge, this is the first report of a study of homopolymers spread as films on any oil/water interface by the SLS technique. We have found that the surface pressure can be calculated from the SLS data because of the decoupling of the longitudinal waves from the transverse capillary waves. The dynamic surface pressure thus obtained agreed with the static surface pressure determined by the Wilhelmy method over the whole concentration range of PVAc. The transverse viscosity could also be calculated exactly for PEO and PVAc and was found to be close to zero in both cases.

Introduction

Interfacial activity of a water-soluble polymer, poly(ethylene oxide) (PEO), is an interesting subject[1,2] which also commands significant technological implications because many nonionic surfactants contain the ethylene oxide moiety. Although experiments with spread films of PEO at the air/water interface (henceforth denoted as A/W for short) have been published,[1,2] those on oil/water interfaces are yet to be found in the literature. On the other hand, studies of adsorbed films at O/W as contrasted to spread films have been reported.[3,4] Some reviews[5,6] covering a wide range of surface-active polymers are available in the literature. This is the second[7] in a series of papers comparing surface-active polymeric materials at A/W and at the heptane–water interface (henceforth denoted as O/W) by the surface quasi-elastic light scattering (SLS) technique. The purpose of this paper is twofold. We present the results of SLS experiments, performed at A/W with sufficient precision to allow a quantitative comparison of film elasticities obtained by SLS and the static Wilhelmy plate method. Further, upon making minor optical modifications of the SLS instrument, ready access to the oil/water interface has been accomplished.[7,8] The experiments on homopolymer films at O/W serve to elucidate the advantages and disadvantages of the SLS technique at O/W compared to A/W.

The SLS technique has only begun to be exploited for polymeric films. It has a potential of providing a new set of approaches to polymeric monolayers and films on various interfaces. Recently, there has been an active interest at A/W with respect to small molecule amphiphiles[9-14] such as fatty acids using SLS, but the interpretation of any viscoelastic parameters extracted from SLS is complicated by the various phase transitions and also by the fact that small molecule amphiphile monolayers are inherently less stable than polymer monolayers.[6] Thus, we have also chosen to study poly(vinyl acetate) (PVAc) because it forms stable films of the "expanded type", in addition to PEO for comparison sake.

Some of the questions which must be answered before SLS can be accepted as a well-validated technique deal with the interpretation of viscoelastic parameters; how to compare them with the results of other techniques and deciding which film viscoelastic parameters can actually be extracted by SLS. For film-covered surfaces there is an inherent coupling between the longitudinal (containing shear and dilational components[15]) waves and transverse capillary waves. For film-free liquid interfaces, the capillary wave motion is governed completely by the interfacial tension and the densities and viscosities of the two phases. With a film present, the situation becomes more complicated. An additional film viscoelastic parameter[12] is defined by making the surface tension complex, i.e., $\sigma^* = \sigma - i\omega\mu$, where μ is the transverse surface viscosity and $\omega = 2\pi f_s - i2\pi(\Delta f_{s,c}/2)$, f_s and $\Delta f_{s,c}$ being the frequency shift and corrected frequency full width at half-height, respectively, of the power spectrum of scattered light. Even though the longitudinal waves have a negligible contribution to the light scattering intensity, these waves couple with the transverse capillary waves. The longitudinal waves are governed by a complex elasticity, $\epsilon^* = \epsilon - i\omega\kappa$ where ϵ and κ are the longitudinal elasticity and viscosity, respectively. The longitudinal elasticity ϵ contains a shear component as stated above which cannot be separated

† Permanent address: Department of Industrial Chemistry, Faculty of Engineering, Mie University, Tsu, Mie 514, Japan.

0024-9297/87/2220-2732$01.50/0